Large-Scale Prototype Testing of a Composite Geosynthetics Reinforced Earth Structure for Riverbank Slope Protection Using Fine Grained Sandy Soil

Ulmen Riff L. Circulado[1*] and Glen A. Lorenzo[2]
[1]College of Engineering and Technology
Mindanao State University – Iligan Institute of Technology
Iligan City, 9200 Philippines
[*]*engr.urlc@gmail.com*

[2]Civil Engineering Department
Mindanao State University – Marawi
Marawi City, 9700 Philippines

Date received: September 27, 2019
Revision accepted: January 13, 2020

Abstract

This paper presents the field evaluation of large scale prototypes of an innovative composite geosynthetic reinforced earth (CGRE) structure as an alternative for the conventional earth retaining structures, hence a green engineering design for riverbank slope protection. This reinforced earth structure comprises of a geogrid that serves as the main reinforcement and the cover of the facing member of the structure; and a geotextile as separator medium between the infill soil and intermediate horizontal gravel drainage. Three large scale prototypes at full, half, and no gravel drainage were built, monitored, and tested. Clayey sand soil was the fill material used and a 3/2" to 2" sub-rounded gravel was used for the drainage and facing members. CGRE prototypes were evaluated in saturated conditions, and tested under incremental surcharge loadings with a total applied stress of 40 kPa. Lateral displacements for every layer of the structure were determined using horizontal rods where readings were taken from line gauges. Results showed that prototypes with gravel drainage displaced lower than the permissible limit of 4.0%. The CGRE prototype with full gravel drainage had the smallest average total lateral displacement of 1.28%. Hence, it had a higher interface friction resistance, and pull-out capacity than the one with less or no gravel drainage. Overall, the incorporation of gravel drainage improved the performance of the reinforced earth system by reducing the lateral movements of the structure. Therefore, the CGRE structure is a viable slope protection alternative even under saturated conditions.

Keywords*:* reinforced earth, geogrid, geotextile, lateral displacement, prototype

1. Introduction

For so many years, the use of ripraps, rubbles, and concrete retaining structures were traditional measures for riverbank protection. As stated by Hiller *et al.* (2017), ripraps are an erosion-resistant ground cover of rocks and soils used as protection to subjacent layers against the impact of hydrodynamic forces due to currents and waves. Considering intermittent and inconsistent occurrence of rainfall, and because of the effects of human-induced activities, the behavior of the water in riverbanks fluctuates. Such a recurring phenomenon triggers soil to erode if exposed and not protected. Hence, the stability of the riverbanks is greatly affected by the interaction of water within the soil system. According to Jafarnejad *et al*. (2017), changing atmospheric conditions due to climate change may alter the rate and distribution of precipitation. Such incident influences the time of occurrence, frequency, and magnitude of extreme flood events, which make existing riverbank slope protection structures and flood protection measures like ripraps vulnerable to the risk of failure considering the possible changes in flood regime.

Moreover, because of the development of hydrostatic pressure, reduction of soil cohesion, and scouring, riverbank failures happen inevitably even with the support of ripraps and other retaining structures. The results and findings of the study of Hiller *et al.* (2017) determined that the accumulated displacement within the slope was one of the crucial factors affecting the stability of placed riprap structures on steep slopes. This is an indication that soil structure with significant slope and in contact with water needs reinforcement to restrain the movements of the earth mass in riverbanks, stabilizing the entire slope protection system and therefore, preventing massive erosion and possible mass wasting.

In the Philippines, even with the protection of ripraps used for banks and creeks, structural problems are still encountered, which result in instability and failure of the entire soil system. Further, attributed to riprap failure is soil subsidence or mass wasting that causes detriments and unwanted injuries to the community. It also disrupts the hydraulic regime of the river, which makes such occurrence variable and unpredictable. As reported on local news and as shown in Figure 1, some cases concerning riprap failures were the following.

Figure 1. Slope protection structure failures in Zamboanga City, Philippines on September 13, 2019 – Sinunuc River (a), Lunzuran River (b), and Divisoria-Putik River (c)

On September 13, 2019, in Zamboanga City, floods due to continuous heavy rainfalls destroyed slope protection structures in 12 barangays amounting to a total damage cost of 48 million pesos as reported by the City Engineer's Office of Zamboanga City (Climaco, 2019). Moreover, a year before the incident, the City Engineer's Office submitted another report on riverbank retaining structure damages. The said office showed that damages reached 31.744 million pesos covering a total length of 729 linear meters of slope protection projects in barangays Bolong, Putik, Bunguiao, Ayala, Tugbungan, Guiwan, and Sta. Maria caused by flooding spawned by typhoon Ompong and southwest monsoon (Climaco, 2018). Also, last September 2016 and August 2015, riprap failures and riverbank land subsidence happened in Marikina River. This incident affected almost 100 residences of the said location. More so, in July of 2015, some houses in the relocation site situated near the riverbank of San Jose Del Monte, Bulacan, abruptly collapsed after a riprap structure of the river had failed. Huge roads cracks on the said site were also visible, which posed a threat to the residences thereat. Also, in July of 2015, houses on the creek supported by ripraps at Caloocan City collapsed during heavy rainfall.

In Rodriguez, Rizal, also in July 2015, an abrupt riprap collapse occurred in a riverbank at a government housing project. It resulted in a massive erosion of land measuring at around 3 m in width that caused fear among residents of the said area. Furthermore, last August 2013 in Zamboanga City, the riprap as riverbank protection structure failed due to excessive rainfall causing considerable flood to the four barangays of the said area; thus, forcing the residents to evacuate to a more secure and safe location. The riprap structures were assessed to be not more than five years from the time of construction

(GMA News, 2013, 2015a, 2015b, 2015c, 2015d, 2016). These are some of the many cases of riverbank slope protection failures in the Philippines.

Based on the reports, riverbank and riprap failures took place during or after continuous rainfall, which makes it evident that the excessive contact of water to soil affects the behavior and performance of the earth retaining system. Thus, proper mitigating measures are necessary to avoid future devastating incidents. According to Zornberg (2007), conventional and traditional approaches in mitigating and preventing earth slope failures and soil erosion consist of a concrete retaining wall or a moderately flat unreinforced slope. For the past years, these types of structures were applied as earth retaining structures. Reinforced concrete retaining walls are easy to design, but the construction and materials costs are quite expensive. Sharma and Goliya (2014) stressed that the height of the wall is directly proportional to the cost of concrete retaining structure. Conversely, most projects in which limited area controls the design excluded the building of unreinforced earth structure with flat slopes (Zornberg, 2007). Hence, in every geotechnical engineering endeavor, the design and construction of stable slopes with satisfactory space requirements are of great consideration for land area maximization and economic significance.

Nowadays, geosynthetics reinforced earth walls are widely used and adopted in the construction industry more often because such structures are more economical than the traditional concrete retaining structures. Likewise, it can be constructed with ease, and tolerate large deformation and settlements; it is also flexible in nature and has high load-carrying capability (Guler and Ocbe, 2003; Khan and Saran, 2006; Sharma and Goliya, 2014; Rawi and Abade, 2017). Primarily, the purpose of incorporating geosynthetics in the design is that it allows the building of stable steep slopes and walls at limited space. Riverbank areas usually have limited construction space and considerable wall altitude. Certainly, a geosynthetics earth reinforced system generally provides an optimized cost-space efficient alternative for the design of an earth retaining structure (Zornberg, 2007). Based on previous comparative studies, reinforced earth structures using geosynthetics are deemed more economical than the conventional reinforced concrete retaining and unreinforced structures (Nalawade and Nalawade, 2008; Sharma and Goliya, 2014; Singh and Akhtar, 2015; Rawi and Abade, 2017). Additionally, in determining the effectiveness of reinforced earth design, laboratory experiments and numerical simulations on the behavior of soil-reinforcement interactions were performed by researchers frequently with varying parameters such as the type

of geosynthetics or reinforcement and soil classification (Guler and Ocbe, 2003; Khan and Sharan, 2006; Zornberg, 2007; Balakrishnan and Vishwanadham, 2015; Yu *et al*. 2015; Anubhav and Wu, 2015; Denine *et al*., 2016).

Moreover, as for the large scale field test, most studies have conducted a pullout test performance of the geosynthetics to evaluate the shear resistance of the soil-geosynthetics on field. Also, actual instrumentations of field models were performed where wall deformations and reinforcement strains of the reinforced structures were determined (Abu-Farsakh *et al*., 2006; Benjamin *et al.*, 2007; Ferreira *et al*., 2015; Esmaili and Hatami, 2015). Nonetheless, traditional orientation of the reinforcement and wall facing blocks are still frequently used. Hence, the design of the reinforced earth structures used were of the same typical model as the previously established on field; and as observed, coastal and river application of reinforced earth are not yet fully explored. With this, there is a gap between experimental studies which reveal the viability and flexibility of the geosynthetics for soil reinforcement, and the performance evaluation and validation of such to actual field application.

Furthermore, according to Benjamin *et al.* (2007), the application of geosynthetics has been highly recommended by many for earth reinforced structures. However, due to the lack of data on the field performance of geosynthetics reinforced earth structures, its utilization is constrained in some critical structures. As such, this study developed, designed and constructed large-scale field prototypes of an innovative composite geosynthetics reinforced earth (CGRE) structure that can be used for riverbank slope protection.

At present, according to Reddy, *et al.* (2018), the most established geosynthetics soil retaining system is the mechanically stabilized earth (MSE) or reinforced earth (RE) technique. Because of its flexible features such as embedded reinforcements and wall facing block, there is continuous development on this system for more various applications on geotechnical engineering structures. This system uses geosynthetics as reinforcement for the soil that prevents the facing wall from lateral movement and stabilizes the adjacent backfill soil. With such components and features in the earth system, an innovative slope protection structure using the MSE technique for riverbanks application is a probable green engineering alternative for the traditional reinforced concrete and ripraps retaining structures. Hence, to

strengthen the significant use of reinforced earth structure in various field applications, this study determined and evaluated the viability of an innovative composite system of a geogrid-geotextile reinforced earth structure for riverbank slope protection on a large-scale field prototype testing. Such field evaluation provides invaluable information in understanding the behavior of the model based on actual field performance of the designed prototype (Benjamin *et al.*, 2007).

2. Methodology

2.1 Geosynthetics Properties

The geosynthetics used in this experimental study were geogrid and geotextile manufactured by TenCate Geosynthetics (Figure 2). A geogrid is a uniaxial type Miragrid GX60/30, and geotextile is a continuous filament nonwoven needle-punched type Polyfelt TS50.

Figure 2. TenCate Miragrid GX60/30 and Polyfelt TS50

Table 1 lists the properties of geosynthetic materials. Specifically, the geogrid was the primary reinforcement of the earth retaining system and this geotextile was the separator medium between infill soil and coarse aggregate drainage.

Table 1. Geosynthetic properties (TenCate Geosynthetics)

Miragrid GX60/30		Polyfelt TS50	
Mass per unit area	280 g/m^2	Mass per unit area (g/m^2)	200 g/m^2
Characteristic initial strength	60 kN/m	Thickness (mm)	2.2 mm
		Tensile strength	15 kN/m
Strain at initial strength	10%	Tensile elongation (MD/CD)	75/35 %
Long term design strengths – for clay silt or sand (60 years)	37.6 kN/m)	Effective opening size O_{90}	0.10 mm
		Grab strength (MD/CD)	920/810 N
		Apparent opening size O_{95}	0.21 mm
		Permittivity	2 s^{-1}

2.2 Infill and Backfill Soil Properties

The infill and backfill materials used for the reinforced earth prototypes were sand with fines type of soil. The soil properties were determined and evaluated in the laboratory following the standard of the American Society for Testing and Materials (ASTM). From the physical property tests performed, the soil had a specific gravity of 2.66 (ASTM D 854, 2002), a liquid limit of 45.19%, a plastic limit of 19.08%, and a plasticity index of 26.11%. Moreover, the result from particle size analysis specified that the soil was well-graded with a coefficient of curvature of greater than ten (>10) and a coefficient of gradation of 1.72 (ASTM C 136, 2001; ASTM D 422, 2002). Figure 3 illustrates the particle distribution curve of fill materials.

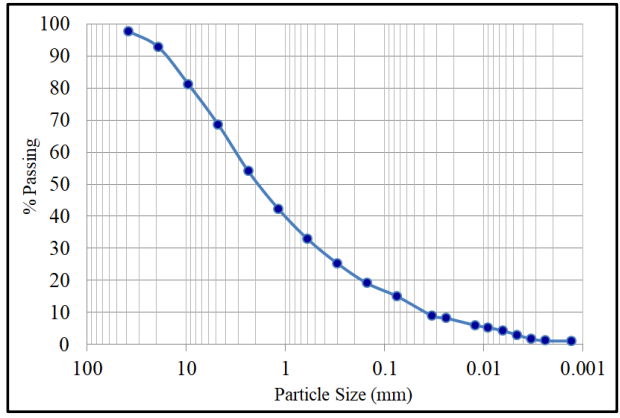

Figure 3. Particle size distribution of infill and backfill soil

Table 2 shows the percent by mass of soil sample, indicating that the primary component of soil was sand particles. Based on the Unified Soil Classification System (USCS) as per ASTM D 2487 (2011), the soil was classified as SC-clayey sand.

Table 2. Percent by mass of soil samples

Type	Size	Percent
Gravel	> 4.75 mm	31.46%
Sand	4.75 mm to 0.075 mm	53.49%
Silt	0.075 mm to 0.005 mm (or 2μm)	12.07%
Clay	< 0.005 mm (or 2μm)	2.98%

The backfill and infill soils were compacted up to its maximum dry density of 1762.5 kg/m^3 with a corresponding optimum moisture content of 18.63%. The compaction test performed was under ASTM D 698 (2000). More so, in evaluating shear strength parameters, the maximum dry density was used in performing direct shear test as per ASTM D 3080 (2003). The normal stresses applied during the direct shear test were 50, 100, and 200 kPa. Figure 4 illustrates the soil friction angle and cohesion intercepts with values of 29.40° and 26.80 kPa, respectively. Table 3 shows a summary of the properties of the infill and backfill soil materials.

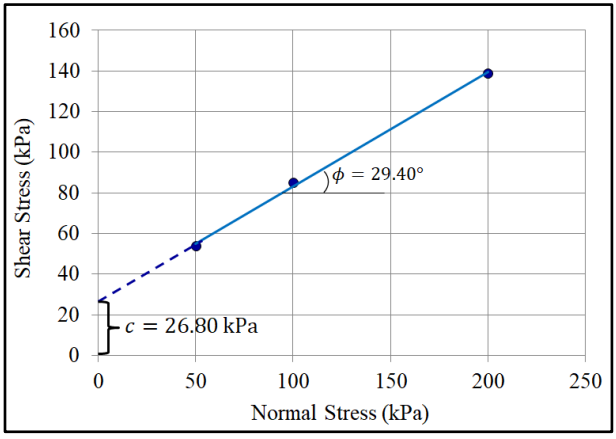

Figure 4. Plot of the normal stress - shear stress of soil

Table 3. Summary of infill and backfill soil properties

Property	Value	Property	Value
Specific Gravity	2.66	Maximum Dry Density	1762.5 kg/m^3
Liquid Limit	45.19%	Optimum Moisture Content	18.63%
Plastic Limit	19.08%	Friction Angle, ϕ	29.40°
Plasticity Index	26.11%	Cohesion	26.80 kPa
		Soil Classification (USCS)	SC-Clayey Sand

2.3 Coarse Aggregate Properties

Coarse aggregate in the form of sub-angular gravel served as intermediate horizontal drainage, which facilitated the release of pore pressures inside the reinforced earth structure. The particle size of gravel ranges from 3/2" to 2" with a specific gravity of 2.72. Also, the loose and compacted densities of the gravel material were 1421.80 kg/m^3 and 1538.41 kg/m^3, respectively. Properties of gravel were determined and evaluated following ASTM C 29 (1997) and ASTM C 127 (2001). Table 4 shows a summary of the properties of the coarse aggregate.

Table 4. Coarse aggregate properties

Property	Value	Property	Value
Specific Gravity	2.72	Loose Density	1,421.80 kg/m^3
Particle Size	3/2" – 2"	Compacted Density	1,538.41 kg/m^3
		Shape	Sub Angular

2.4 Design Overview of the Field Program

For the design of the CGRE wall, the concept and procedures described by Elias *et al.* (2001) and Koerner (2005) were applied. A conservative design for the external stability analysis of the structure was employed, and the factor of safety considered for internal stability was 1.0 – that is, the prototype was designed to carry only its weight; thus, at critical boundary condition. The purposes of such were to assess the behavior of the CGRE model and establish the displacement curves of each prototype when evaluated under the fully saturated condition, which was further subjected to surcharge loadings. The coefficient of shear stress interaction for geogrids used for the design of the

CGRE prototype was from the technical specifications established by TenCate Geosynthetics, with values ranging from 0.70 to 0.80 for clayey soil sand. The design computations for the composite reinforced earth prototype resulted in a geogrid reinforcement length of 0.90 m and a uniform spacing of 0.40 m. The height of the prototype is 2.4 m, with a length of 1.80 m and a width of 1.20 m. Figure 5 illustrates the schematic diagram of the prototype.

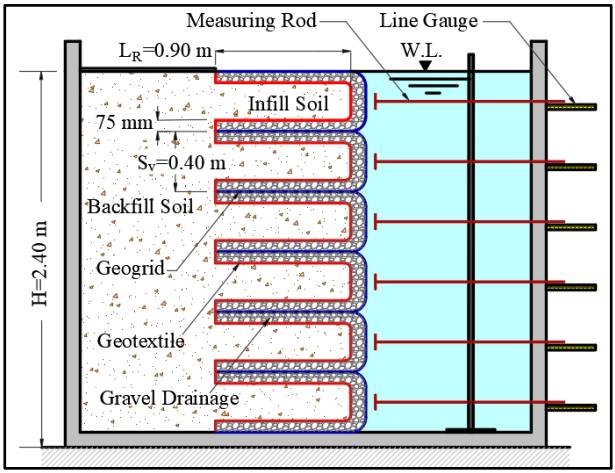

Figure 5. Schematic diagram of the large-scale prototype setup

Table 5 delineates the computational design requirements for the CGRE model.

Table 5. Design requirements of the CGRE model

Phase 1: Requirements for External Stability	
Sliding	$FS_{sliding}=\frac{\sum \text{Horizontal Resistance Forces}}{\sum \text{Horizontal Sliding Forces}}\geq 1.5$
Overturning	$FS_{overturning}=\frac{\sum \text{Resisting Moment}}{\sum \text{Driving Moment}}\geq 2.0$
Bearing Capacity	$FS_{bearing}=\frac{q_{ult}}{q_{actual}}\geq 2.0$
Phase 2: Requirements for Internal Stability	
Tensile Failure	$FS_{rupture}=\frac{T_{allow}}{T_{max}}$
Pullout Failure	$FS_{pullout}=\frac{T_{pullout}}{T_{max}}$

where:

$$T_{allow} = \frac{T_{ult}}{CRF} = \frac{T_{ult}}{RF_{CR} \times RF_{ID} \times RF_{CD} \times RF_{BD}}$$

$$T_{max} = K\sigma_v S_v \left(FS_{eq}\right)$$

$$T_{pullout} = 2C_i C_r L_e \sigma_v \tan \phi'_{fill}$$

T_{allow}= allowable tensile strength
T_{max}= maximum tensile strength
$T_{ultimate}$= ultimate tensile strength
$T_{pullout}$= pullout strength
RF= reduction factor
σ_v= vertical earth pressure
C_i= pullout interaction coefficient
C_r= covergae ratio
K= earth pressure coefficient
L_e= effective length of embedment
ϕ'_{fill}= friction angle of filling material

2.5 Field Test Setup

The large-scale CGRE prototype was comprised of multi-function elements such as an integrated facing wall barrier, composite reinforcements, and layers of an intermediate horizontal drainage system. The geogrid served as the primary reinforcement and as a cover-barrier of the facing member of the CGRE structure. The geotextile worked as a separator medium for the infill soil and intermediate horizontal gravel drainage, and as a secondary reinforcement. For this experimental study, three large scale prototypes were built, monitored, and tested at full-gravel drainage of 0.90 m, half-gravel drainage of 0.45 m, and no-gravel drainage. The intermediate horizontal gravel drainage thickness was 75 mm for all prototypes. Figure 6 shows the three prototypes with varying intermediate horizontal gravel drainages.

The construction and testing of field prototypes were conducted in a rectangular reinforced concrete tank with a size of 2.60 m height, 3.0 m length, and 1.50 m width. Figures 7a and 7b illustrate the actual dimensions of the test tank.

Additionally, since the spacing of geogrid reinforcement was at 0.40 m, six layers of composite reinforced members with a total height of 2.40 m were constructed on the actual site. In supplying and draining water inside the tank, a water system was installed with piping inlet and outlet connections attached to an onsite water reservoir.

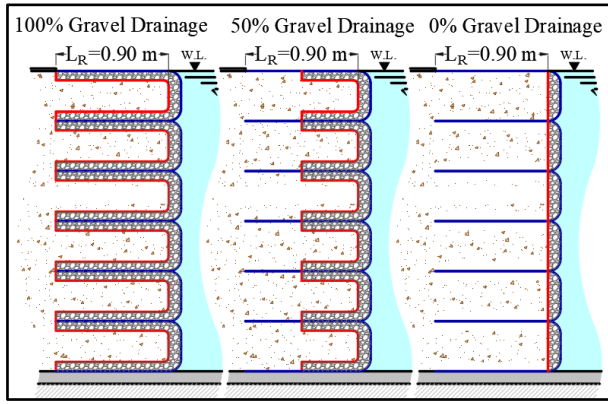

Figure 6. Three CGRE prototypes with varying intermediate horizontal gravel drainage

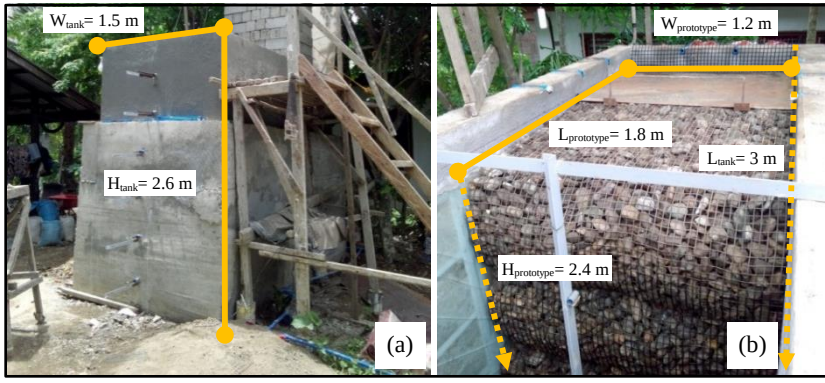

Figure 7. Actual prototype test tank (a) and isometric view (b)

2.6 Instrumentation

Horizontal rods placed at the center of every layer of the prototype inside the tank and extended through the exterior walls were used to evaluate lateral displacements. Line gauges outside the tank were installed to determine displacement readings. Figures 5 and 8 illustrate the schematic diagram and the actual installation of horizontal rods with line gauges, respectively.

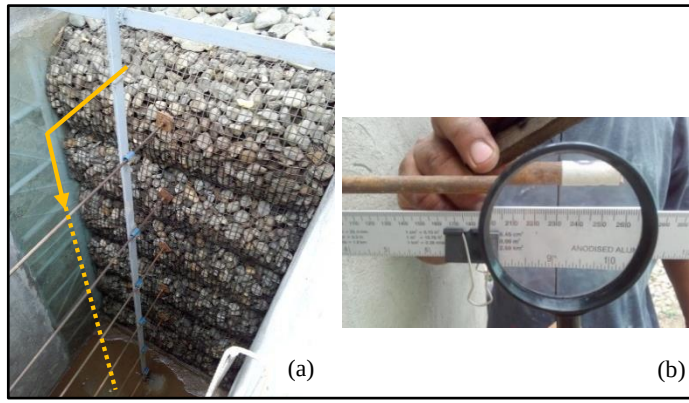

Figure 8. Actual setup of measuring rods (a) and close-up view of line gauge (b)

2.7 Construction of Large-scale Prototype

Backfill and infill soil materials were prepared at optimum moisture content of 18.63%, and then weighed and packed at targeted quantity based on the maximum dry density of 1762.5 kg/m^3. Soil materials were manually compacted using a fabricated steel-concrete tamper of 20 kg weight, and at a constant drop height of 400 mm. Compaction effort of 600 kN-m/m^3 was maintained throughout the construction of the three prototypes as per ASTM D 698 (2000). Gravel was rodded to achieve the maximum compacted density of 1,538.41 kg/m^3 following ASTM C 127 (2001). Figures 9a and 9b show the actual compaction of the backfill and infill soils and rodding of the gravel layer.

Figure 9. Soil compaction (a) and gravel rodding (b)

At the onset of the construction, a temporary facing board was installed to support and restrain the CGRE structure from any early horizontal movement. Removal of the said temporary structure followed after the construction of the final layer. Moreover, the systematic procedures for the construction of large-scale prototypes were the following: first, geogrid was placed below the foundation interface, which served as the first layer of reinforcement and protective cover of the reinforced earth system; then, the placement of coarse aggregate gravel with a thickness of 75 mm followed. The succeeding procedure was the installation of geotextile with infill soils compacted uniformly. After the compaction of fill materials, the geotextile was laid on top of the compacted soils to cover it. After which, coarse aggregates gravel was placed on top of the geotextile and at facing section with geogrid as protective cover and reinforcement. The same process was repeated throughout the construction of the six composite layers until the prototype height reached a height of 2.4 m. Figure 10 shows the main components of the prototype during the construction phase (Figure 10a). Furthermore, Figure 10b shows the final layer of the prototype, where a steel plate with dimensions of 1.20 m width and 0.90 m in length was placed and leveled on top in preparation for the application surcharge loading.

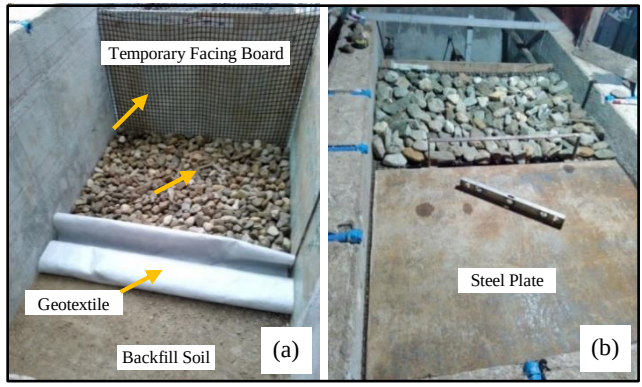

Figure 10. Components of the composite reinforced earth prototype during construction phase (a) and prototype at the final layer (b)

2.8 Prototype Testing

At the end of the construction (EOC) of the prototypes, initial readings of the lateral displacement were taken and recorded. Subsequently, the test tank was supplied with water until the reinforced earth system was fully immersed

(Figure 11). The prototype was then soaked for 24 hours (h) to achieve a full-saturation state. Afterwards, the water inside the test tank was drained; and then, the second lateral displacement readings at fully saturated conditions (FSC) were recorded.

Figure 11. Prototype fully immersed inside the test tank

The second phase of prototype testing was performed with the application of incremental surcharge loading. The total applied stress induced in the CGRE system was 40 kPa of 14 layers of concrete blocks. The lateral displacement readings were recorded for every two layers of concrete blocks at 3 h interval, with the prototype being submerged with water. This procedure was repeated seven times until the full surcharge load of 40 kPa was applied. Figure 12 shows the total surcharge loading induced on top of the CGRE prototype.

After the completion of the full-gravel drainage testing, the succeeding evaluations were performed for half-gravel drainage and no-gravel drainage conditions while considering all parameters constant and construction procedures the same.

Figure 12. Full surcharge load of 40 kPa
applied in the prototype

3. Results and Discussion

3.1 EOC Lateral Displacement of the CGRE Prototypes

Lateral displacements of the CGRE prototypes were determined using measuring rods and line gauges located in the middle section of every layer of the reinforced earth facing member. The recorded measurements were in millimeters which were further normalized for presentation. Normalization was made for the structure height and lateral displacement in relation to the total height of the wall. Hence, the expression for the said displacement was in percentage; and a normalized unit of 1 defined the total height of the prototype (Ravichandra *et al.*, 2018). The American Association of State Highway and Transportation Officials (AASHTO) and the Federal Highway Administration (FHWA) guidelines presented horizontal facing deformations in the percentage of $\Delta x/H$ (Bathurst *et al.*, 2014).

At the EOC, the extreme points, which were the top and bottom layers, had relatively high displacements compared to the intermediate points for the three

setups. The bottom layers yielded the highest lateral displacement with percentage values of 1.03, 2.10, and 2.26% for prototypes 1, 2, and 3, respectively. Nevertheless, for the intermediate members, the maximum displacement occurred in the middle third portion of the structure. For prototype 1 (full-gravel drainage setup) and prototype 2 (half-gravel drainage setup), the maximum intermediary displacement occurred at 0.42H with percentage values of 0.80 and 1.54%, respectively. As for the prototype 3 (no-gravel drainage setup), the maximum intermediary displacement occurred at 0.58H with a percentage value of 1.46%. Figure 13 illustrates the EOC lateral displacement graph of prototype 1.

Prototypes 1 and 2 had similar displacement behavior showing decreasing non-linear curve paths from the maximum intermediary point. Conversely, prototype 3 also showed a non-linear curve path, but the location of the maximum intermediary point was at the upper middle third portion of the structure. Furthermore, the average lateral displacements of the three prototypes at EOC were 0.69, 1.43, and 1.46%, respectively, with prototype 1 yielding the lowest value. Prototypes 2 and 3 had a comparable horizontal displacement.

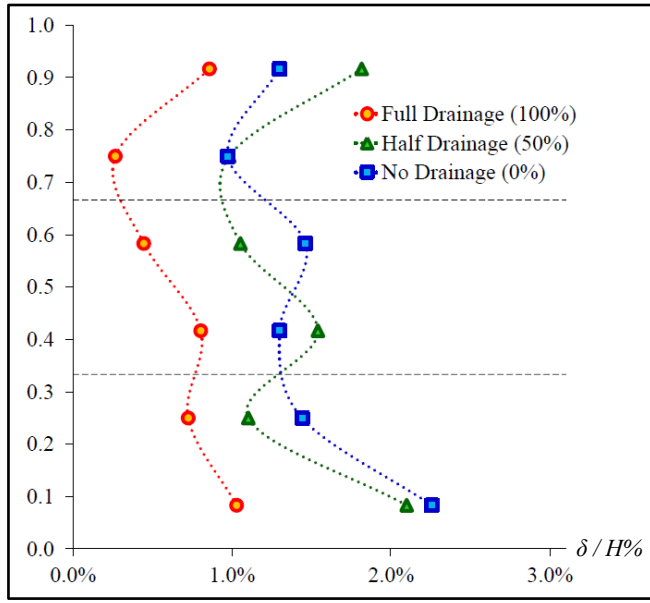

Figure 13. Normalized lateral displacement vs. prototype height at EOC

3.2 Lateral Displacement of the CGRE Prototypes at FSC

Moisture content determination for every layer of the CGRE model was conducted to assess the saturation state of the prototypes. Based on the results of the test, all layers of the three prototypes achieved a fully saturated condition after 24 h immersion to water.

Lateral displacements behavior of prototypes under FSC were determined and evaluated to delineate the reaction of the CGRE prototypes with the interaction and infiltration of water to the system. Figure 14 shows that changes took place on the initial positions of the reinforced members after the immersion of prototypes in water for 24 h. Considering average lateral displacements, prototype 1 had the lowest displacement with a percentage value of 1.24%, which is significantly lower than the two prototypes, followed by prototype 2 (1.67%) and then prototype 3 (1.87%). Prototypes 2 and 3 had comparable displacements.

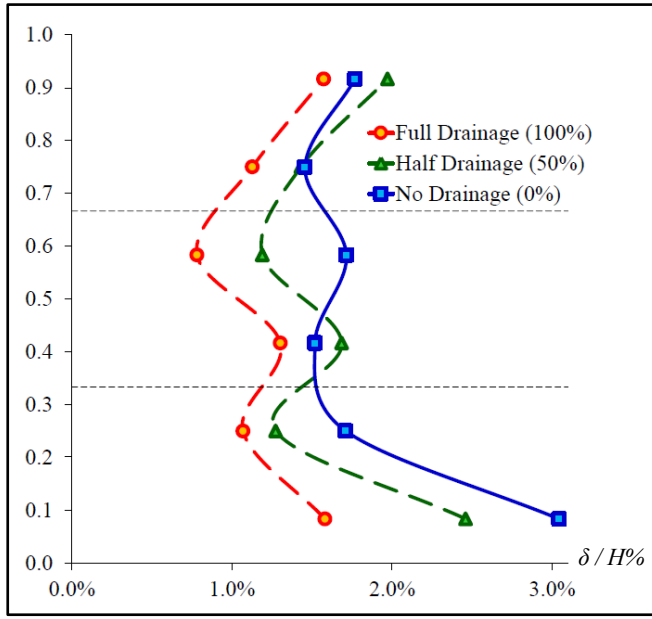

Figure 14. Normalized lateral displacement vs. prototype height at FSC

In evaluating the lateral displacement behavior of the prototypes under FSC, the pattern for the displacement curve of the three prototypes remained consistent with the EOC observations, that is, extreme points had relatively

high displacements as compared to the intermediate points. Also, maximum intermediary points were all located in the middle section of the structure with decreasing non-linear curve paths. The location of the maximum intermediary point for prototypes 1 and 2 was at 0.42H, and for prototype 3, it was at 0.58H with percentage values of 1.30, 1.69, and 1.72%, respectively. Moreover, the highest lateral displacement at FSC occurred at the bottom layers for all prototypes having percentage values of 1.58, 2.46, and 3.05% for prototype 1, 2, and 3, respectively.

3.3 Lateral Displacement of the CGRE Prototypes at Total Surcharge Loading (TSL)

At the final phase of this study, vertical surcharge loading of 40 kPa in the form of concrete blocks was applied in the system. This applied stress was twice as much as the capacity of the designed CGRE structure. From the result of the test at TSL, a slight movement in position had occurred from FSC, and the graph pattern of the displacement behavior remained consistent with only minor changes. Figure 15 illustrates the lateral displacement curves of the prototypes at total surcharge loading.

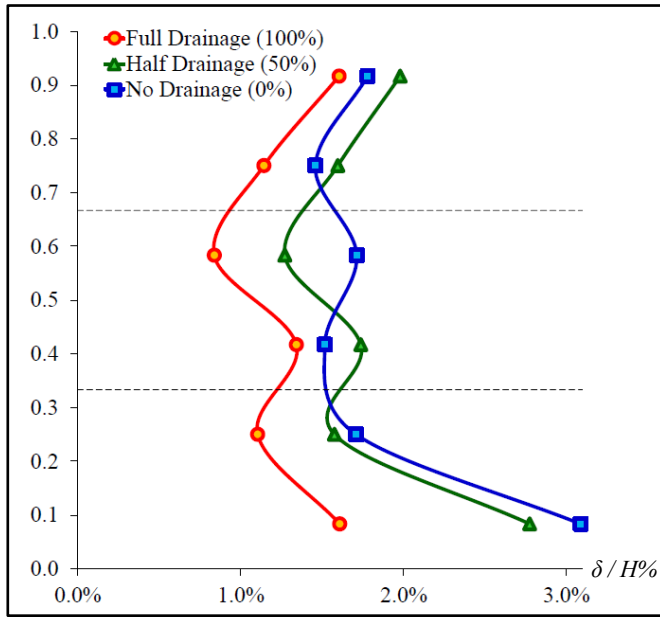

Figure 15. Normalized lateral displacement vs. prototype height at TSL

Additionally, from the evaluations made, prototypes 1 and 2 had similar non-linear curve paths with their maximum intermediary point lying on the middle third of the structure, specifically at 0.42H. The percentage value of the maximum intermediary point for prototypes 1 and 2 was 1.35 and 1.74%, respectively. Prototype 3 also had a non-linear curve path having maximum intermediary point at 0.58H and with a percentage value of 1.72%. Also, for the extreme sections of the prototypes, the bottom layer yielded the highest later displacement relative to other points in the CGRE structure. The displacement percentage values at the bottom layer for prototypes 1, 2, and 3 were 1.61, 2.78, and 3.09%, respectively.

Considering the average lateral displacement of the CGRE structures in the final position, prototype 1 had the lowest displacement value of 1.28%, which is significantly smaller than the percent displacements of the two prototypes. Conversely, prototypes 2 and 3 had average lateral displacements of 1.83 and 1.88%, which were comparable to each other.

3.4 Displacement Behavior of Individual CGRE Prototypes

As shown in Figure 16, prototype 1 (full-gravel drainage setup) had a significant movement in position from EOC to FSC. The maximum change in displacement occurred at 0.75H, with a deviation of 0.86%.

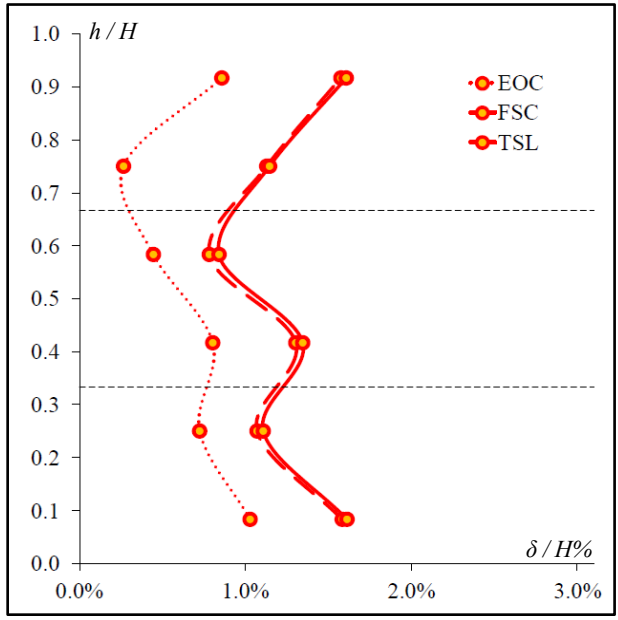

Figure 16. Displacement behavior of prototype 1 (Full-gravel drainage)

On average scale, the deviation from EOC to FSC was observed to be 0.55%, while no significant movement in positions occurred from FSC to TSL. The maximum and average deviations were only 0.06 and 0.04%, respectively. Moreover, the maximum and minimum total deviations from EOC to TSL were 0.88% at 0.75H, and 0.38% at 0.25H, respectively. The average total deviation was 0.59%, with a change factor of 1.85 from EOC to TSL.

Prototype 2 (half-gravel drainage setup) had a gradual movement in position from EOC to FSC, and from FSC to TSL. The maximum change in displacement from EOC to FSC occurred at 0.75H with a deviation of 0.45%. However, the observed maximum movement from FSC to TSL and the total maximum change from EOC to TSL were at the bottom section of the structure with deviation values of 0.32 and 0.68%, respectively. Considering intermediary points, the maximum and minimum total change in displacement occurred at 0.75H and 0.42H with deviation values of 0.62 and 0.20%, respectively. Furthermore, the average total deviation from EOC to TSL was 0.39% with a change factor of 1.27. Figure 17 illustrates the displacement behavior of prototype 2.

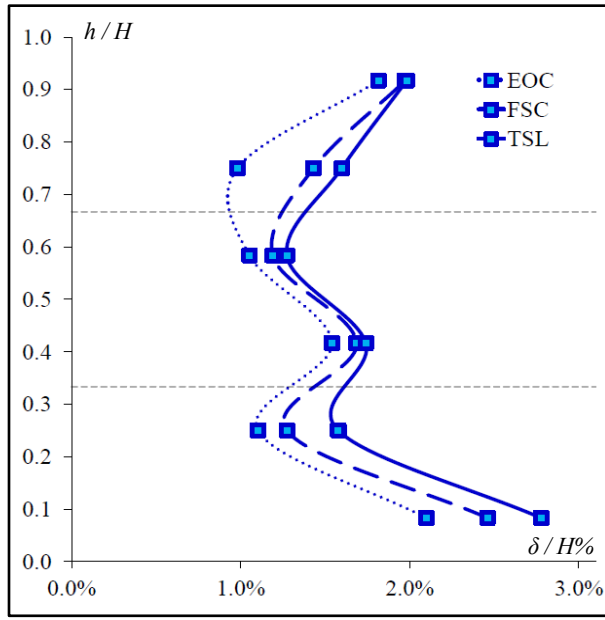

Figure 17. Displacement behavior of prototype 2
(Half-gravel drainage)

In evaluating the displacement behavior of prototype 3 (no-gravel drainage setup), the layer position movements took place from EOC to FSC, with a maximum deviation of 0.79% occurring at the bottom layer. The average deviation from EOC to FSC was 0.41%. However, there was no noticeable change in layer positions that occurred from FSC to TSL. The observed movements were evident in the upper and lower sections; no change in layer positions was noticed in the intermediary points. The average deviation from FSC to TSL was only 0.01%. Considering the total change in layer positions from EOC to TSL, the location of the maximum and minimum deviations were at the bottom layer and at 0.42H with percentage values of 0.83 and 0.22%, respectively. The average change factor from EOC to TSL was 1.29. Figure 18 shows the graphical illustration of the displacement behavior of prototype 3.

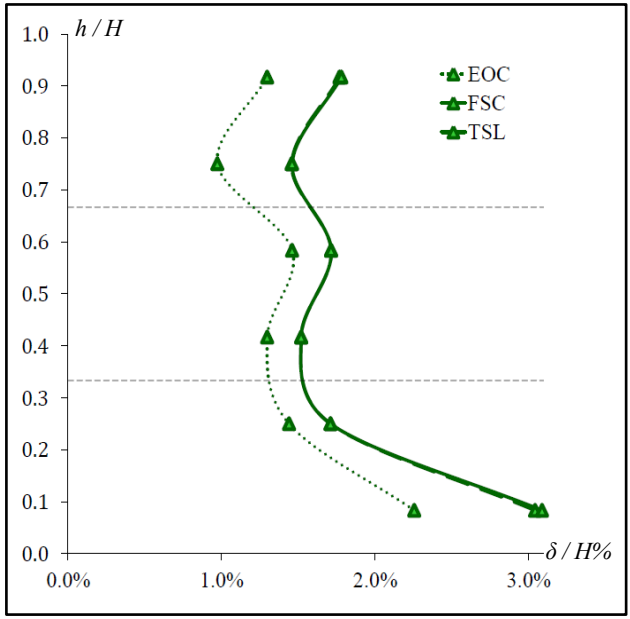

Figure 18. Displacement behavior of prototype 3
(No-gravel drainage)

4. Conclusion

The maximum total displacement of the three prototypes occurred at the bottom layer of the structure, with prototype 3 having the highest percent

displacement of 3.09%, while prototype 1 had the lowest with 1.61% displacement. This indicates that sliding at the bottom section happened, and that the prototype with full-gravel drainage setup had a much higher interface friction resistance than the prototypes with less or no gravel drainage. Moreover, a noticeable movement had occurred at the upper layer of the three prototypes from the initial to the final position. This gives a notion that the anchorage design and reinforcement strength on the topmost section must be taken into consideration to restrain the upper layer from any possible active movement. In evaluating the intermediary layers of the three prototypes, the location of the maximum displacement occurred in the middle-third section of the structure, specifically at 0.42H for prototypes 1 and 2, and at 0.58H for prototype 3. Prototypes with gravel drainage had similar displacement behavior curves. A structure bulging of the CGRE structure was the evident behavior observed, especially for prototypes with gravel drainage.

Additionally, it was evident that there were significant changes in position that happened from EOC to FSC, indicating that the action of water into the system influences the displacement behavior of every layer of the CGRE prototypes. Furthermore, no significant changes in position occurred from FSC to TSL, which implied that the design of the reinforced earth wall was satisfactory.

Considering average lateral displacement, prototype 1 had the lowest total lateral displacement but the highest deviation. On the other hand, prototypes 2 and 3 had a comparable total displacement and deviation values. Nevertheless, prototype 2 had lower displacement and deviation than prototype 3. The incorporation of gravel drainage significantly contributes to a better structural performance of the reinforced earth structure. Therefore, given that the main function of drainage is to release water pressure in an earth retaining system, the incorporation of intermediate gravel drainage in the reinforced earth structure improves the performance of the said structure by reducing any possible lateral movement. The gravel drainage acted as a secondary reinforcement, which resulted in a much higher pull-out resistance because of the coarse aggregates in between intermediate layers. Finally, the individual and average percent displacements of the prototypes with gravel drainage were lower than the permissible limit of 4% as per the guidelines established by AASHTO and FHWA.

5. References

American Society for Testing and Materials (ASTM) C 29/C 29M-97. (1997). Standard test method for bulk density ("unit weight") and voids in aggregate. West Conshohocken, PA: ASTM International.

American Society for Testing and Materials (ASTM) C 127-01. (2001). Standard test method for density, relative density (specific gravity), and absorption of coarse aggregate. West Conshohocken, PA: ASTM International.

American Society for Testing and Materials (ASTM) C 136-01. (2001).Standard test method for sieve analysis of fine and coarse aggregates. West Conshohocken, PA: ASTM International.

American Society for Testing and Materials (ASTM) D 422-63 R02. (2002). Standard test method for particle-size analysis of soils. West Conshohocken, PA: ASTM International.

American Society for Testing and Materials (ASTM) D 698-00. (2000). Standard test methods for laboratory compaction characteristics of soil using standard effort (600 kN-m/m^3). West Conshohocken, PA: ASTM International.

American Society for Testing and Materials (ASTM) D 854-02. (2002). Standard test methods for specific gravity of soil solids by water pycnometer. West Conshohocken, PA: ASTM International.

American Society for Testing and Materials (ASTM) D 2487-11. (2011). Standard practice for classification of soils for engineering purposes (unified soil classification system). West Conshohocken, PA: ASTM International.

American Society for Testing and Materials (ASTM) D 3080-03. (2003). Standard test method for direct shear test of soils under consolidated drained conditions. West Conshohocken, PA: ASTM International.

Abu-farsak, M.Y., Almohd, I., & Farrag, K. (2006). Comparison of field and laboratory pullout test on geosynthetics in marginal soils. Transportation Research Record: Journal of the Transportation Research Board, 1975, 124-136. https://doi.org/10.1177%2F0361198106197500114

Anubhav, & Wu, H. (2015). Modeling of non-linear shear displacement behavior of soil-geotextile interface. International Journal of Geosynthetic and Ground Engineering, 1(19), 1-10. https://doi.org/10.1007/s40891-015-0021-7

Balakrishnan, S., & Viswanadham, B.V.S. (2015). Performance evaluation of geogrid reinforced soil walls with marginal backfills through centrifuge model tests. Geotextiles and Geomembranes, 44(1), 1-14. https://doi.org/10.1016/j.geotexmem.2015.06.002

Bathurst, R.J., Miyata, Y., & Allen, T.M. (2010). Facing displacement in geosynthetic reinforced soil walls. In: Finno, R., Hashash, Y.MA., Arduino, P. (Eds.), Proceedings of the 2010 Earth Retention Conference. ASCE-Geo-Institute, Bellevue, Washington, United States, 442-459.

Benjamin, C.V.S., Bueno, B.S., & Zornberg J.G. (2007). Field monitoring evaluation of geotextile-reinforced soil-retaining walls. Geosynthetics International, 14(2), 100-118. https://doi.org/10.1680/gein.2007.14.2.100

Climaco, B. [Beng]. (2018, September 2). Infra damage due to ompong soars to P49.9m [Facebook status update]. Retrieved from https://m.facebook.com/story/graphql_permalink/?graphql_id=UzpfSTk2NjY2MzAzMDEzOjEwMTU1OTI3MTI4ODI4MDE0

Climaco, B. [Beng]. (2019, September 25). CEO reports P48M infra damage due to flooding [Facebook status update]. Retrieved from: https://web.facebook.com/bengclimaco/photos/pcb.10156756946878014/10156756944573014/?type=3&theater

Denine, S., Della, N., Muhammed, R.D., Feia, S., Canou, J., & Dupla J.C. (2016). Effect of geotextile reinforcement on shear strength of sandy soil: laboratory study. Studia Geotechnica et Mechanica, 38(4), 1-13. https://doi.org/10.1515/sgem-2016-0026

Elias, V., Christopher, B.R., & Berg, R.R., (2001). Mechanically stabilized earth walls and reinforced soil slopes: design & construction guidelines. FHWA-NHI-00-043, Federal Highway Administration, Washington, DC.USA. Retrieved from http://www.fhwa.dot.gov>nhi10024

Esmaili, D., & Hatami, K. (2015). Meared performance and stability analysis of large-scale reinforced model embankments at different moisture content. International Journal of Geosynthetics and Ground Engineering, 1(22), 3-16. https://doi.org/10.1007/s40891-015-0024-4

Ferreira, F.B., Vieira, C.S., Lopes, M.L., & Carlos, D.M. (2015). Experimental investigation on the pullout behaviour of geosynthetics embedded in a granite residual soil. European Journal of Environmental and Civil Engineering, 20(9), 1-34. https://doi.org/10.1080/19648189.2015.1090927

GMA News. (2016, September 26). QRT: Riprap sa boundary ng Marikina at San Mateo, Rizal, gumuho. [Video File]. Retrieved from https://www.youtube.com/watch?v=VsT7jB2Y8TY

GMA News. (2015a, August 31). 24Oras: Halos 100 pamilya, pinalikas matapos gumuho ang ilang bahay sa gilid ng Marikina River. [Video File]. Retrieved from https://www.youtube.com/watch?v=6LQzPJ9cSNM

GMA News. (2015b, July 10). Tatlong bahay sa relocation site, gumuho nang bumigay ang riprap [Video File]. Retrieved from https://www.youtube.com/watch?v=TSsRx2ZuuSI

GMA News. (2015c, July 9). 24Oras: Riprap sa pabahay ng gobyerno sa Rodriguez, Rizal, gumuho matapos mistulang lamunin ng tubig [Video File]. Retrieved from https://www.youtube.com/watch?v=KukW_lwvQiQ

GMA News. (2015d, July 9). UB: Pundasyon ng 5 bahay na nakatayo malapit sa creek sa Caloocan, gumuho [Video File]. Retrieved from https://www.youtube.com/watch?v=dGEkzLr6ypw

GMA News. (2013, August 5). Oras: Ilang barangay sa Zamboanga City, lubog sa baha matapos gumuho ang riprap [Video File]. Retrieved from https://www.youtube.com/watch?v=r-q8fsnEydc

Guler, E., & Ocbe, C. (2003). Centrifuge and full-scale models of geotextile reinforced walls and several case studies of segmental retaining walls in Turkey. Emirates Journal for Engineering Research, 8(1), 15-23.

Hiller, P.H. Aberle, J., & Lia, L. (2017). Displacements as failure origin of placed riprap on steep slopes. Journal of Hydraulic Research, 56(2), 141-155. https://doi.org/10.1080/00221686.2017.1323806

Jafarnejad, M., Pfister, M., Brűhwiler, E., & Scheiss, A.J. (2017). Probabilistic failure analysis of riprap as riverbank protection under flood uncertainties. Stochastic Environmental Research and Risk Assessment, 31, 1839-1851. https://doi.org/10.1007/s00477 016-1368-6

Khan, I.N., & Saran, S. (2006). A model study in metallic strip-reinforced earth wall. Malaysian Journal of Civil Engineering, 18(1), 38-45.

Koerner, R.M. (2005). Designing with Geosynthetics (5th Ed.). Pearson Prentice Hall, Upper Saddle River, NJ 07458: Pearson Education, Inc.

Nalawade, R.D., & Nalawade, D.R. (2008). Stability and cost aspects of geogrid reinforced earth wall of flyover. International Association for Computer Methods and Advanced in Geomechanics, 1-6.

Rawi, O.A., & Abade M.A. (2017) Design of geo-synthetic retaining walls as an alternative to the reinforced concrete walls in Jordan. American Journal of Engineering Research, 6(12), 301-312.

Ravichandra, A.P., Madhav, M.R., Narasimha Reddy, G.V., & Padmavathi, V. (2018). Performance of model gabion type retaining walls built using cylindrical cells: A laboratory study. International Journal of Geosynthetics and Ground Engineering, 4(18). https://doi.org/10.1007/s40891-018-0135-9

Reddy, M.M., Reddy, K.R.S., & Asadi, S.S. (2018). An experimental study on combination of geosynthetic material with sand for evaluation of shear strength parameters. International Journal of Pure and Applied Mathematics, 119(4), 1779-1786. https://doi.org/10.13140/RG.2.2.28463.18086

Sharma, M., & Goliya, H.S. (2014). Design and economic analysis of reinforced earth wall. International Journal of Emerging Trends in Engineering and Development, 4(6), 172-188.

Singh, H., & Akhtar, S. (2015). A review on economic analysis of reinforced earth wall with different types of reinforcing materials. International Journal of Latest Technology in Engineering, Management & Applied Science, 4(12), 68-74.

Yu, Y., Bathurst, R.J., & Miyata, Y. (2015). Numerical analysis of a mechanically stabilized earth wall reinforced with steel strips. Soils and Foundations, 55(3), 536-547. http://dx.doi.org/10.1016/j.sandf.2015.04.006

Zornberg, J.G. (2007). New concepts in geosynthetic-reinforced soil. Proceedings of the Fifth Brazilian Symposium on Geosynthetics, Geossinteticos 2007 and of the Sisxth Brazilian Congress on Environmental Geotechnics. Recife, Brazil, 1-26.